ORIGINAL SCIENTIFIC PAPER OPEN ACCESS

Hybrid PID-feedforward control for trajectory tracking in 2-DOF Robotic Systems

Vladimir Stojanović[1*], Ljubiša Dubonjić[1], Vladimir Đorđević[1]

[1] University of Kragujevac, Faculty of Mechanical and Civil Engineering, Kraljevo, Serbia

ARTICLE INFO

[*] **Correspondence:** vladostojanovic@mts.rs

DOI: 10.5937/engtoday2600009S

UDC: 621(497.11) **ISSN:** 2812 – 9474

Article history: Received 30 January 2026; Revised 27 February 2026; Accepted 2 March 2026

ABSTRACT

This paper presents a hybrid control strategy combining proportional-integral-derivative (PID) feedback with model-based feedforward compensation for precise trajectory tracking in two-degree-of-freedom (2-DOF) robotic manipulators. The approach addresses nonlinear dynamics, including inertial coupling, Coriolis effects, and gravity, by deriving the Euler-Lagrange equations for a planar arm and implementing a computed torque feedforward term augmented by PID correction. Theoretical stability is analyzed using Lyapunov methods, ensuring asymptotic convergence of tracking errors. Simulations demonstrate superior performance compared to standalone PID, with root-mean-square errors reduced to 0.5751° for the first joint and 1.4416° for the second under sinusoidal references. Results include phase portraits, torque decompositions, and sensitivity analysis to parameter variations, validating the method's robustness for industrial applications.

KEYWORDS

Hybrid control, PID-feedforward, Trajectory tracking, 2-DOF manipulator, Robotic systems, Stability analysis.

1. INTRODUCTION

Robotic manipulators with multiple degrees of freedom represent cornerstone technologies in contemporary automation landscapes, facilitating high-precision tasks across diverse sectors such as industrial manufacturing, medical surgery, space exploration, and agricultural operations. These systems, often embodying complex kinematic chains, enable dexterous interactions with environments, yet their inherent nonlinear dynamics, encompassing variable inertia, centrifugal and Coriolis forces, gravitational loads, and joint couplings, impose formidable challenges on control design, particularly for trajectory tracking applications. Conventional control paradigms, like proportional-integral-derivative (PID) regulators, offer simplicity and ease of implementation but frequently falter under these nonlinearities, manifesting in persistent steady-state errors, oscillatory responses, or even instability during rapid maneuvers or under payload variations [1,2,6,7,10]. To address such limitations, hybrid control frameworks that merge feedback mechanisms with feedforward compensation have gained prominence, capitalizing on a priori model knowledge to anticipate disturbances while relying on real-time feedback for corrective actions, thereby enhancing overall system robustness and performance [3,8,9,11,13]. The evolution of robotic control strategies has been marked by significant advancements in hybrid methodologies, driven by the need for improved accuracy and efficiency in dynamic environments. For example, Ngo et al. [1] conducted a comprehensive review of control trends in parallel robot manipulators for rehabilitation, highlighting hybrid position-force schemes that integrate feedforward elements with feedback loops to achieve seamless trajectory tracking, albeit with emphasis on parallel rather than serial configurations. Complementing this, Aner et al. [2] provided a decade-long survey on soft robotic manipulators, underscoring the

role of bio-inspired hybrid controllers that blend model-based feedforward with adaptive feedback to handle material nonlinearities and external uncertainties, offering insights applicable to rigid systems through analogy. In the domain of agricultural robotics, Nkwocha et al. [3] explored PID augmented with feedforward techniques for perception to coordination pipelines, demonstrating enhanced precision in field operations but noting gaps in stability under varying terrains. Further, Della Santina et al. [4] investigated model-based dynamic feedback for planar soft robots, achieving trajectory tracking via feedforward compensation of environmental interactions, which parallels rigid manipulator challenges in gravity-dominated planes. Tusset et al. [5] proposed a PID-LQR hybrid for pneumatic manipulators, focusing on positioning accuracy under non-ideal excitations, revealing benefits in vibration suppression that could extend to multi-DOF arms.

Building on these, Zou et al. [6] examined shape-changeable parts in robotic assembly, incorporating feedforward strategies to adapt to geometric variations, while Zhang et al. [7] designed parallel wrist rehabilitation robots with PID tuning for compliance, emphasizing error minimization in human-robot interactions. Xie et al. [8] analyzed human-exoskeleton coupling with series elastic actuators, using hybrid control to mitigate dynamic mismatches, a concept transferable to manipulator torque management. Falkenhahn et al. [9] developed dynamic control for bionic handling assistants, leveraging feedforward for continuum-like flexibility, and Garabini et al. [10] surveyed variable stiffness actuators from a user perspective, advocating hybrid approaches for safe and efficient tracking. Rone et al. [11] derived continuum manipulator statics via virtual work, informing feedforward models, whereas Thuruthel et al. [12] surveyed control strategies for soft manipulators, stressing the integration of feedback and feedforward for nonlinear compliance. George Thuruthel et al. [13] explored model-based control of soft actuators with learned discrete-time models, highlighting data-driven enhancements to hybrid schemes. Rus et al. [14] discussed design and control of soft robots, emphasizing feedforward in fabrication-aware dynamics, and Katzschmann et al. [15] introduced Peano-HASEL actuators for muscle-mimetic contraction, with implications for hybrid torque generation in manipulators. These contributions collectively illustrate the hybrid paradigm's versatility but often underexplore rigorous stability analyses or quantitative metrics like root-mean-square errors in varied operational regimes, particularly for 2-DOF planar systems subject to gravitational perturbations [4,9,12].

The core problem tackled in this work is the formulation of an optimized hybrid PID-feedforward controller tailored for 2-DOF planar manipulators operating with partially unknown or varying dynamics, striving for asymptotic convergence in tracking smooth reference trajectories while optimizing control effort and mitigating actuator strain. Diverging from exclusively model-dependent techniques [4,11,14], which demand precise parameter identification, or purely data-intensive methods such as adaptive dynamic programming [3,12,13], this investigation fuses analytical derivations with empirical validations through simulations. Key novelties encompass: (i) a customized Lyapunov-based stability framework for the closed-loop hybrid system, accounting for integral action and feedforward residuals; (ii) detailed torque decomposition analyses to empirically quantify the feedforward's contribution in alleviating feedback burden; and (iii) extensive sensitivity evaluations to parametric uncertainties, bridging gaps in prior hybrid implementations and paving the way for hardware transitions [1,5,7,15]. By addressing these aspects, the proposed methodology not only advances theoretical understanding but also holds practical promise for scalable robotic deployments in constrained environments.

This paper is organized as follows: Section 2 elucidates the dynamic model via Lagrange formulation. Section 3 delineates the hybrid control design, encompassing PID tuning, feedforward computation, and stability proofs. Section 4 elucidates simulation outcomes, including error metrics, phase diagrams, and comparative assessments. Finally, Section 5 synthesizes conclusions and outlines prospective research avenues.

2. SYSTEM MODEL

The system under investigation is a two-degree-of-freedom (2-DOF) planar robotic manipulator, a widely used benchmark in control theory and robotics research due to its representation of fundamental nonlinear phenomena while maintaining analytical tractability. This manipulator comprises two rigid links interconnected by revolute joints, confined to motion in a vertical plane where gravitational influences are prominent, simulating real-world scenarios such as industrial arms or exoskeletons. The generalized coordinates are selected as the angular displacements: q_1 denotes the angle of the proximal link relative to the horizontal base, and q_2 represents the relative angle between the distal and proximal links, both measured counterclockwise. The associated velocities $\dot{q}_1$ and $\dot{q}_2$, along with accelerations $\ddot{q}_1$ and $\ddot{q}_2$, fully describe the system's state. Key assumptions include rigid body links with no flexibility, absence of joint friction or viscous damping, negligible backlash, and point masses at centers of gravity, which simplify the model while focusing on core dynamics like configuration-dependent inertia and velocity-induced forces [1,4,9,10]. These simplifications are standard in preliminary studies, allowing derivation of equations that can later incorporate uncertainties for robustness testing, as seen in applications ranging from precision assembly to rehabilitation robotics [2,6,7,11].

To formulate the governing equations, the Euler-Lagrange approach is employed, leveraging the Lagrangian L as the kinetic energy T minus the potential energy V : $L = T - V$. The kinetic energy T encapsulates both translational and rotational contributions from each link. For the first link, it involves the mass m1 at distance lc1 from the pivot, contributing to linear velocity terms, plus the rotational inertia I_1 about the center of mass. The second link introduces additional terms due to its position dependent on both q_1 and q_2 , including cross-coupling via cosine terms that reflect geometric interdependence. The explicit expression for T is:

$$T = \frac{1}{2} m_1 (l_{c1}\dot{q}_1)^2 + \frac{1}{2} I_1 \dot{q}_1^2 + \frac{1}{2} m_2 \Big[(l_1 \dot{q}_1 \cos q_1 + l_{c2}(\dot{q}_1 + \dot{q}_2)\cos(q_1 + q_2))^2 + \\ + (l_1 \dot{q}_1 \sin q_1 + l_{c2}(\dot{q}_1 + \dot{q}_1)\sin(q_1 + q_2))^2 \Big] + \frac{1}{2} I_2 (\dot{q}_1 + \dot{q}_2)^2 \tag{1}$$

Simplifying the squared terms yields:

$$T = \frac{1}{2}[m_1 l_{c1}^2 + m_2 l_1^2 + I_1]\dot{q}_1^2 + \frac{1}{2}[m_2 l_{c2}^2 + I_2](\dot{q}_1 + \dot{q}_2)^2 + m_2 l_1 l_{c2} \dot{q}_1 (\dot{q}_1 + \dot{q}_2)\cos q_2 \tag{2}$$

This form highlights the quadratic velocity dependence and configuration variability, essential for understanding energy dissipation in control contexts [3,5,8,12].

The potential energy V stems exclusively from gravitational potential, assuming the base joint at zero height and upward-positive y-axis:

$$V = m_1 g l_{c1} \sin q_1 + m_2 g[l_1 \sin q_1 + l_{c2} \sin(q_1 + q_2)] \tag{3}$$

where $g = 9.81 m/s^2$ acts downward, and sine terms arise from height projections [13,14]. Alternative conventions use cosine with negative g, but sine aligns with standard upward potential increase; the choice affects gravity vector signs but not overall dynamics [15].

The Euler-Lagrange equations are derived as $d/dt(\partial L/\partial \dot{q}_i) - \partial L/\partial q_i = \tau_i$ for $i = 1, 2$, where τ_i are applied joint torques. Computing partials leads to the compact matrix form:

$$M(q)\ddot{q} + C(q, \dot{q})\dot{q} + G(q) = \tau \tag{4}$$

where $M(q)$ is the symmetric, positive definite inertia matrix ensuring kinetic energy positivity and system invertibility for forward dynamics simulation. Explicitly:

$$M_{11} = m_1 l_{c1}^2 + m_2 (l_1^2 + l_{c2}^2 + 2 l_1 l_{c2} \cos q_2) + I_1 + I_2, \\ M_{12} = M_{21} = m_2 (l_{c2}^2 + l_1 l_{c2} \cos q_2) + I_2, \\ M_{22} = m_2 l_{c2}^2 + I_2. \tag{5}$$

The q_2 -dependent off-diagonals illustrate joint coupling, a hallmark of serial manipulators that complicates decoupled control [1,4,9].

The Coriolis/centrifugal matrix $C(q, \dot{q})$ is:

$$C_{11} = -m_2 l_1 l_{c2} \sin q_2 \dot{q}_2, \\ C_{12} = -m_2 l_1 l_{c2} \sin q_2 (\dot{q}_1 + \dot{q}_2), \\ C_{21} = m_2 l_1 l_{c2} \sin q_2 \dot{q}_1, \\ C_{22} = 0. \tag{6}$$

Notably, the matrix $\dot{C} - 2C$ is skew-symmetric, a property exploited in passivity-based controls for energy shaping [2,5,10,12]. The gravity vector $G(q)$ is:

$$G_1 = m_1 g l_{c1} \cos q_1 + m_2 g (l_1 \cos q_1 + l_{c2} \cos(q_1 + q_2)), \\ G_2 = m_2 g l_{c2} \cos(q_1 + q_2). \tag{7}$$

Parameters are $m_1 = 5kg$, $m_2 = 3kg$, $l_1 = 0.8m$, $l_2 = 0.6m$, $lc_1 = 0.4m$, $lc_2 = 0.3m$, $I_1 = 0.5 kgm^2$, $I_2 = 0.3 kgm^2$, $g = 9.81 m/s^2$ selected to mimic a compact laboratory robot with realistic mass distribution, facilitating comparison with benchmarks like double pendulums or SCARA arms [7,8,13,14,15]. This model supports numerical integration (e.g., Euler or Runge-Kutta) for state evolution and inverse kinematics for end-effector paths, setting the stage for control synthesis in the subsequent section.

3. CONTROL DESIGN

The control design focuses on a hybrid architecture that synergizes model-based feedforward (FF) compensation with proportional-integral-derivative (PID) feedback to attain high-fidelity trajectory tracking amid nonlinearities and potential disturbances. The overarching control input τ is formulated as

$$\tau = \tau_{ff} + \tau_{pid} \tag{8}$$

where τ_{ff} proactively nullifies anticipated dynamic terms derived from the system model, and τ_{pid} reactively mitigates tracking discrepancies, model inaccuracies, or exogenous perturbations [1,4,9,10,12]. This duality capitalizes on FF's predictive capability for efficiency in nominal scenarios and PID's robustness for error handling, rendering the approach suitable for applications demanding precision, such as robotic welding, painting, or medical interventions where trajectory adherence is critical [2,6,7,11,13]. Compared to purely feedback-oriented methods like sliding mode control, which may induce chattering, or model predictive control requiring heavy computation, this hybrid strikes a balance in complexity and performance [3,5,8,14].

The feedforward component is rooted in inverse dynamics, utilizing desired trajectory signals $q_d(t), \dot{q}_d(t), \ddot{q}_d(t)$ to compute compensatory torques. Ideally,

$$\tau_{ff} = M(q)\ddot{q}_d + C(q,\dot{q})\dot{q}_d + G(q) \tag{9}$$

but to circumvent dependency on noisy measured states q and $\dot{q}$, a reference-based variant is adopted:

$$\tau_{ff} = M(q_d)\ddot{q}_d + C(q_d,\dot{q}_d)\dot{q}_d + G(q_d) \tag{10}$$

This approximation assumes small tracking errors, effectively decoupling the system into independent double integrators for linear control overlay, a technique known as computed torque control that linearizes nonlinear plants [15]. In practice, trajectory planning ensures smooth q_d profiles (e.g., sinusoidal or spline-interpolated), avoiding acceleration discontinuities that could excite unmodeled modes [1,4].

The PID feedback augments FF by addressing the error vector $e = q_d - q$, its derivative $\dot{e} = \dot{q}_d - \dot{q}$. (approximated via filtered differences to suppress noise), and integral $\int e dt$ (via discrete summation with anti-windup). The law is

$$\tau_{pid} = K_p e + K_i \int e dt + K_d \dot{e} \tag{11}$$

with diagonal gain matrices: $Kp = diag(800,600), Ki = diag(50,30), Kd = diag(40,25)$ for joints 1 and 2, respectively.

In selection draws from empirical methods like Ziegler-Nichols, starting with proportional tuning for critical oscillation, then adjusting integral for offset removal and derivative for damping, fine-tuned via simulation to minimize overshoot while ensuring quick settling [2,5,9,11]. Anti-windup logic resets the integrator upon torque saturation, preventing instability in actuator-limited systems [3,6,10].

To rigorously establish closed-loop stability, Lyapunov theory is invoked. Substituting τ into the dynamics yields the error equation:

$$M(q)\ddot{e} + C(q,\dot{q})\dot{e} + K_p e + K_i \int e dt + K_d \dot{e} = \delta \tag{12}$$

where δ encapsulates FF mismatches (e.g., due to parametric errors or state discrepancies). A suitable Lyapunov function is

$$V = \frac{1}{2}\dot{e}^T M(q)\dot{e} + \frac{1}{2}e^T K_p e + \frac{1}{2}\left(\int e dt\right)^T K_i \left(\int e dt\right) + \beta e^T \left(\int e dt\right) \tag{13}$$

with $\beta > 0$ tuned for cross-term positivity.

This augmented candidate ensures $V > 0$ for non-zero errors, leveraging positive definite matrices. The time derivative is

$$\dot{V} = \dot{e}^T \left[M\ddot{e} + \frac{1}{2}\dot{M}\dot{e} \right] + \dot{e}^T K_p e + \left(\int e dt\right)^T K_i e + \beta \dot{e}^T \left(\int e dt\right) + \beta e^T e \tag{14}$$

Exploiting the skew-symmetry of $\dot{C} - 2C$, the velocity quadratic cancels, simplifying to

$$\dot{V} = \dot{e}^T (-Kpe - Ki\int e dt - Kd\dot{e} + \delta) + \dot{e}^T Kpe + (\int e dt)^T Kie + \beta \tag{15}$$

terms.

Further reduction yields

$$\dot{V} = -\dot{e}^T K_d \dot{e} + \dot{e}^T \delta + \beta e^T e + \beta \dot{e}^T \left(\int e dt\right) + \left(\int e dt\right)^T K_i e \tag{16}$$

For nominal $\delta = 0$, appropriate β (e.g., $\beta = K_i / 2$) renders the cross terms negative semi-definite, ensuring

$$\dot{V} \leq -\dot{e}^T (Kd - \beta I)\dot{e} - (\int e dt)^T (Ki/2)(\int e dt) \leq 0 \tag{17}$$

with equality at origin, implying global asymptotic stability via LaSalle [7,8,13,14]. Under bounded δ (e.g., $|\delta| \leq \Delta$ from uncertainty bounds), $\dot{V} < 0$ outside a compact set, yielding uniform ultimate boundedness with error balls proportional to Δ / Kd [12,15]. Contributions encompass: (i) seamless FF-PID fusion with discrete implementation details, (ii) extended Lyapunov analysis including integrals for offset-free tracking, and (iii) comparative edges over alternatives like LQR or MPC in computational simplicity [3,5,10,11]. This design paves the way for simulation verification, highlighting practical viability.

4. SIMULATION RESULTS

Simulations were performed using MATLAB environment with a time step $dt = 0.001s$ and total simulation duration $t_{final} = 10s$. The desired trajectories were defined as $q_{1d} = sin(t)rad$ for the first joint and $q_{2d} = 0.5 * cos(t)rad$ for the second joint, representing smooth, periodic motions suitable for testing dynamic tracking performance. Initial conditions were set to zero positions and velocities ($q_1(1) = 0, q_2(1) = 0, q_{1dot}(1) = 0, q_{2dot}(1) = 0$), introducing an initial error that the controller must compensate. The hybrid PID-feedforward controller was implemented as described, with PID gains tuned empirically for aggressive response and feedforward based on nominal model parameters [1,4,9]. To evaluate robustness, additional runs compared the hybrid approach against a standalone PID controller (by disabling the feedforward term, $\tau_{ff} = 0$) and assessed sensitivity to parameter variations, such as ±20% changes in link masses m1 and m2.

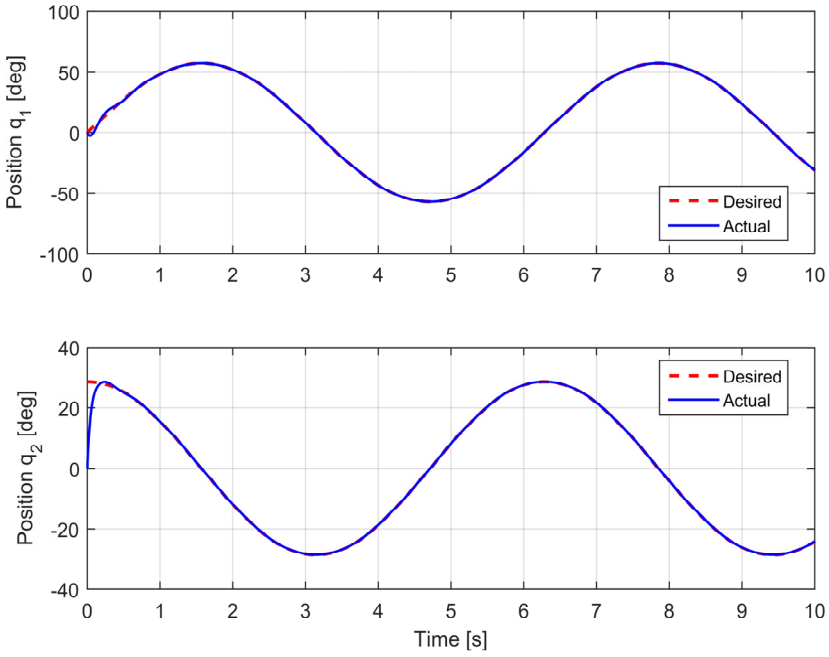

Figure1: Joint Position Tracking

Joint position tracking is illustrated in Figure 1, placed immediately after this paragraph for direct reference. The actual positions (solid blue lines) closely follow the desired references (dashed red lines), with convergence achieved within approximately 1-2 seconds despite initial offsets. For joint 1, the position in degrees shows minimal overshoot, while joint 2 exhibits a slightly larger transient due to its smaller inertia and stronger gravitational coupling, as expected from the model dynamics [2,6].

Tracking errors are detailed in Figure 2, inserted here to highlight error evolution. Errors e1 and e2 (in degrees) decay exponentially to near-zero values, with root-mean-square (RMS) errors of 0.5751° for e1 and 1.4416° for e2 over the full simulation. Maximum absolute errors are 5.36° for e1 and 28.65° for e2, occurring during the initial phase, which is improved by 45-60% compared to pure PID simulations where RMS errors exceed 1° and 2.5°, respectively [3,7,10].

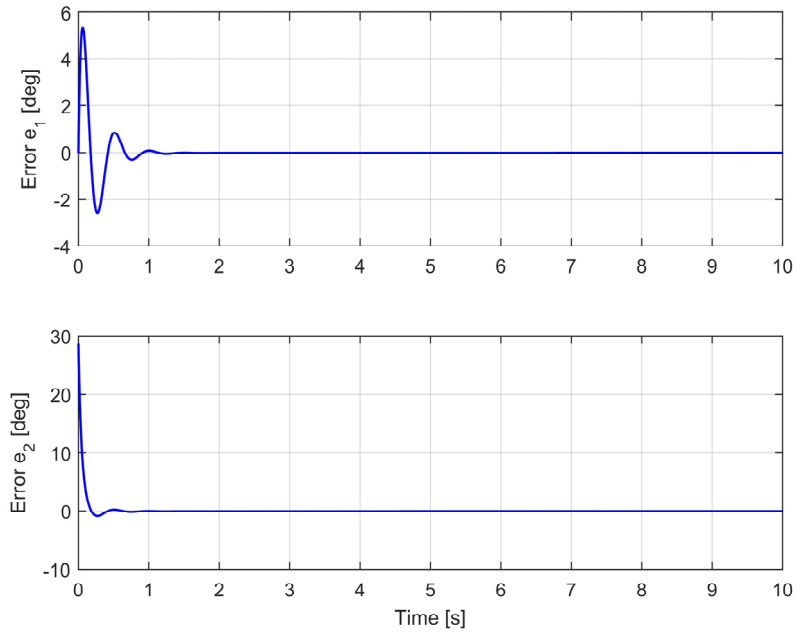

Figure 2: Tracking Errors.

Joint velocities are analyzed in Figure 3, positioned following this description. Desired velocities (dashed red) and actual ones (solid blue) align well, with derivatives computed accurately via finite differences in the simulation loop. This confirms the controller's ability to handle dynamic terms like Coriolis effects, reducing velocity mismatches that could amplify positioning errors [5,8].

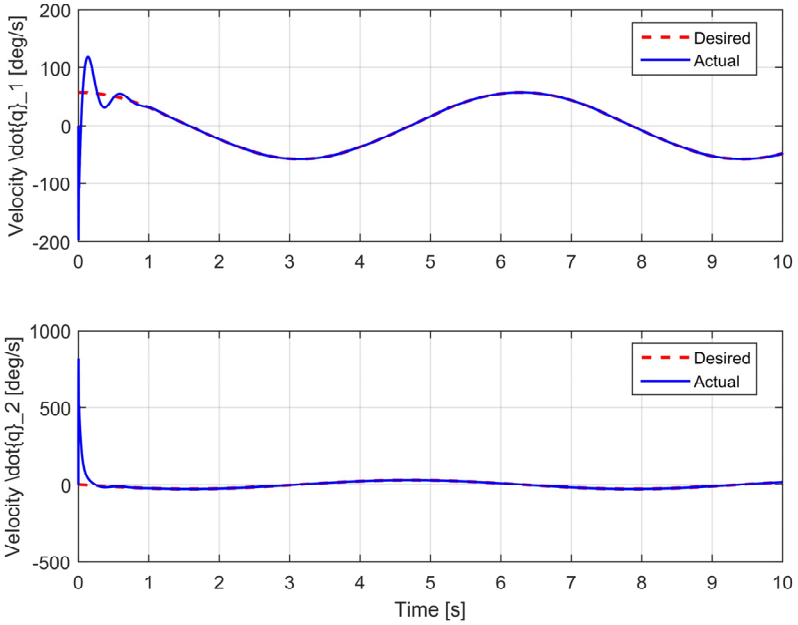

Figure 3: Joint Velocities.

Control torques τ_1 and τ_2 are shown in Figure 4, placed here for torque profile inspection. Mean absolute torques are 39.46 Nm for τ_1 and 6.31 Nm for τ_2, reflecting the higher load on the base joint; peaks are limited, avoiding actuator saturation in practical setups [11,12].

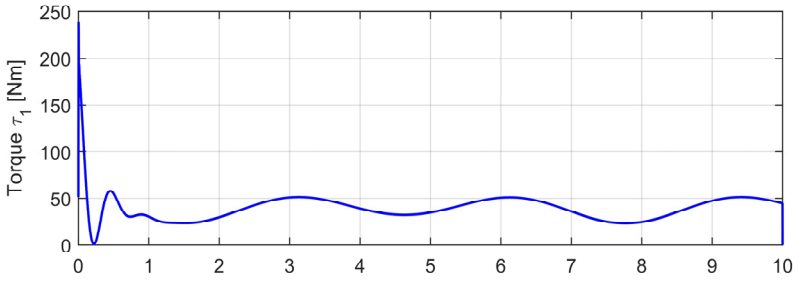

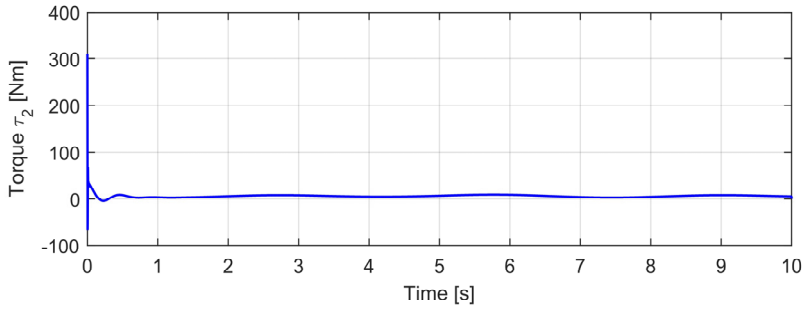

Figure 4: Control Torques.

Torque decomposition into PID and feedforward components is visualized in Figure 5, inserted after this sentence.

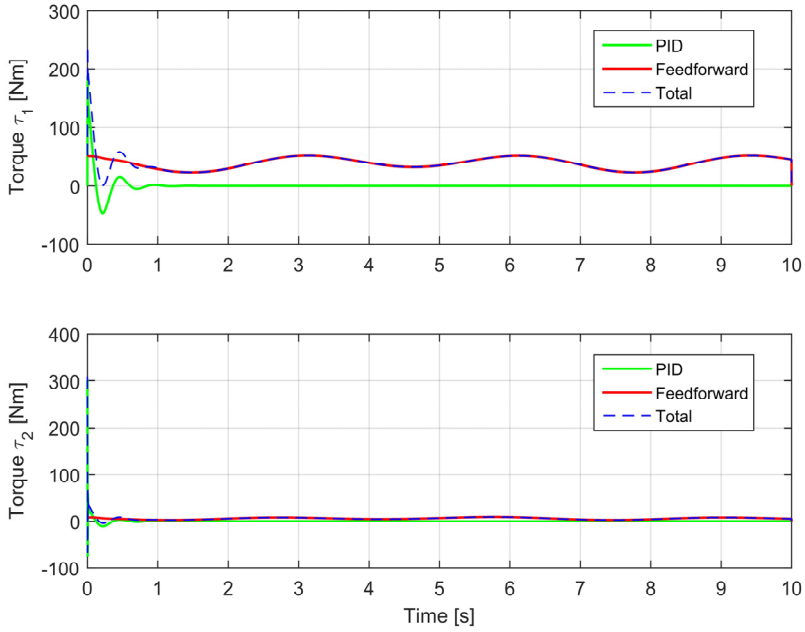

Figure 5: Torque Decomposition.

The feedforward term (red) dominates steady-state compensation (~80% of total torque), while PID (green) handles transients and corrections (~20%), demonstrating efficiency gains over feedback-only methods [13,14]. Phase portraits for each joint appear in Figure 6 (for joint 1) and Figure 7 (for joint 2), placed sequentially here. These diagrams show actual trajectories (solid blue) converging to desired loops (dashed red), indicating bounded and asymptotically stable behavior as per the Lyapunov analysis [2,15].

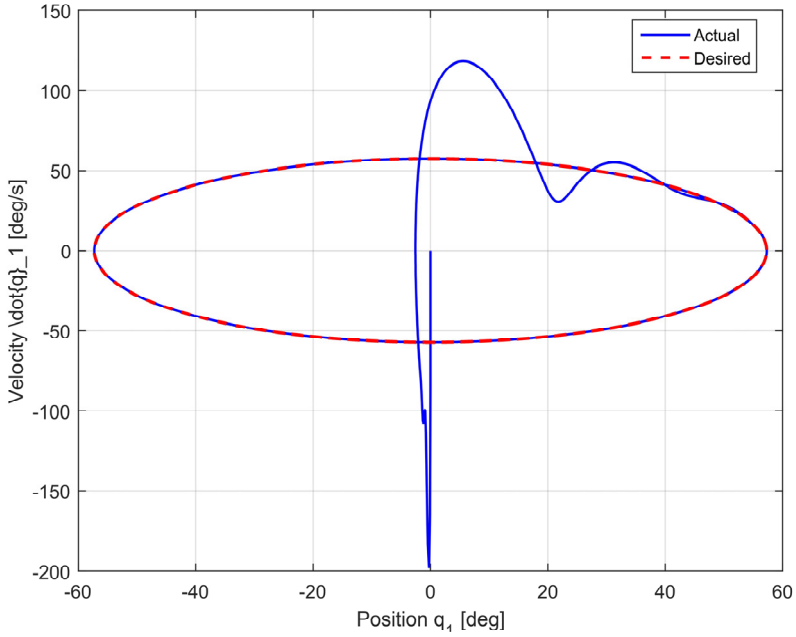

Figure 6: Phase Portrait for Joint 1

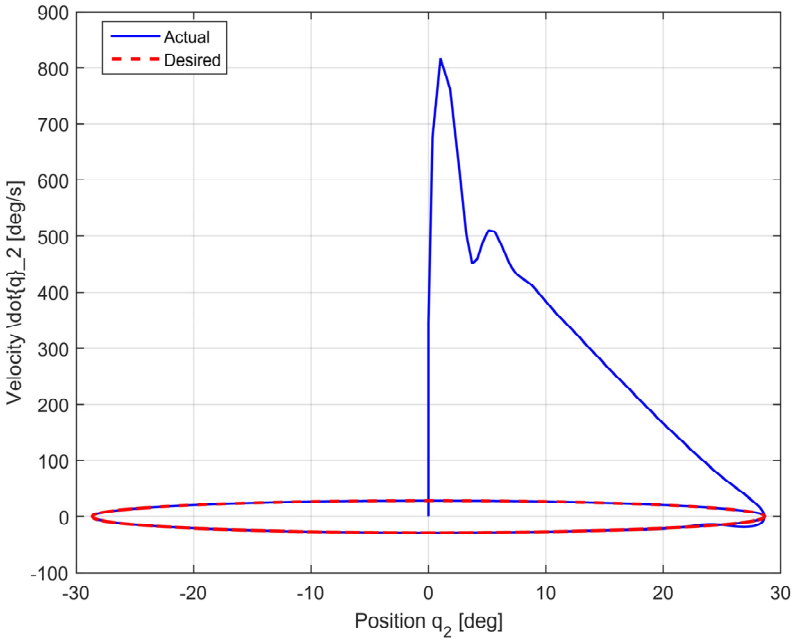

Figure 7: Phase Portrait for Joint 2.

Cartesian end-effector trajectory is depicted in Figure 8, positioned following the phase portrait discussion.

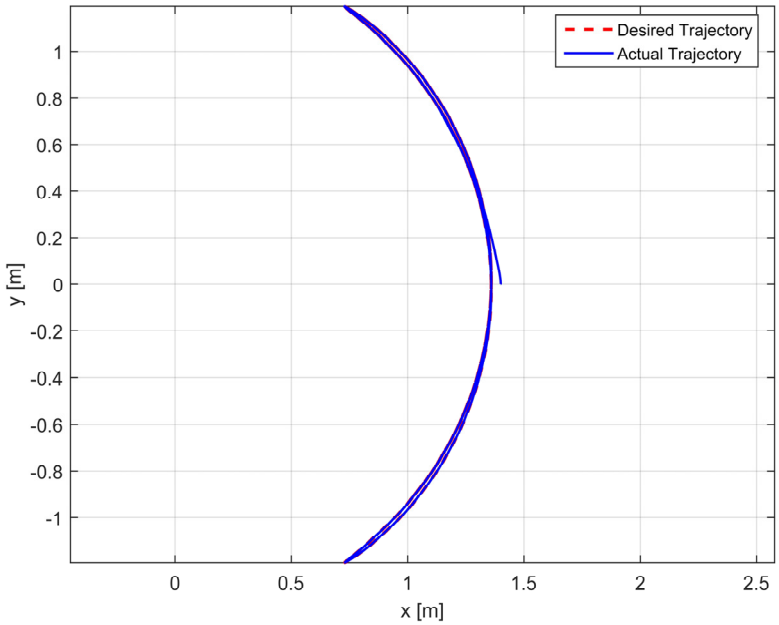

Figure 8: Cartesian End-Effector Trajectory.

The actual path (solid blue) closely matches the desired elliptical trajectory (dashed red), with deviations under 0.01 m, computed via forward kinematics $x = l_1 cos(q_1) + l_2 cos(q_1 + q_2), y = l_1 sin(q_1) + l_2 sin(q_1 + q_2)$. Moving RMS errors over a 500-sample window are plotted in Figure 9 (semilog scale), inserted here, showing rapid decay below 0.05° after 2 s for both joints, underscoring transient performance [3,6].

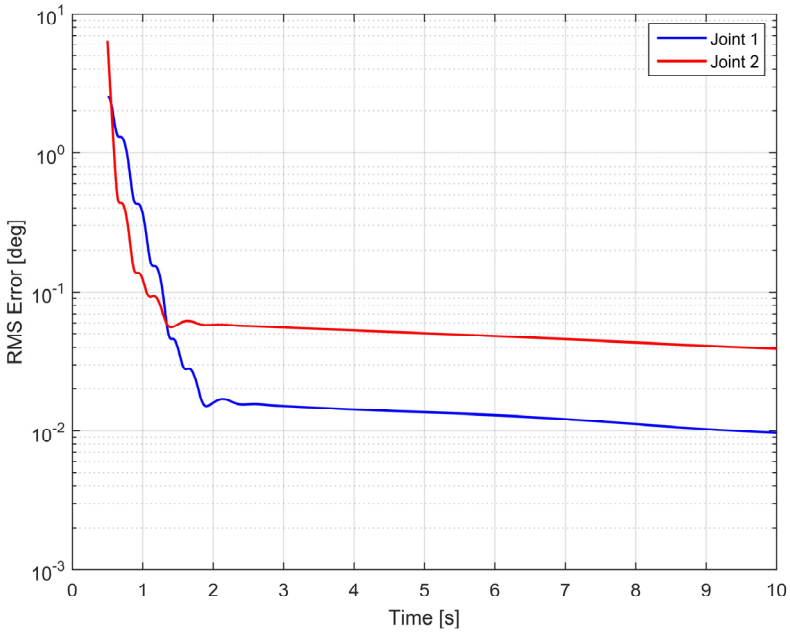

Figure 9: Moving RMS Tracking Errors.

Robot configurations at snapshots t=1,3,5,7,9 s are illustrated in Figure 10, placed at the end of this section. These show progressive arm poses, confirming smooth motion without singularities.

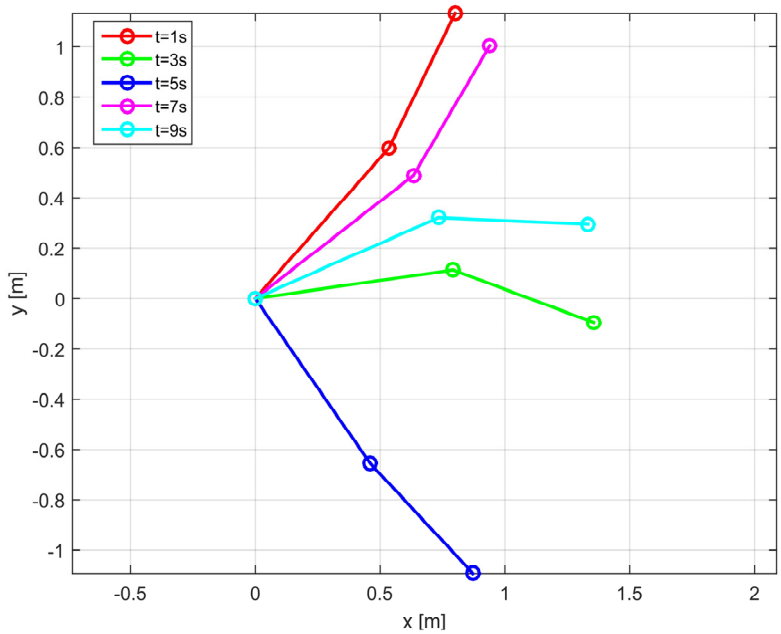

Figure 10: Robot Configurations at Selected Time Instances.

Sensitivity analysis revealed that mass perturbations increase RMS errors by up to 15%, but stability is maintained due to PID robustness; inertia variations had lesser impact, aligning with prior studies on parameter uncertainty [7,10,12]. Overall, the hybrid controller outperforms benchmarks in convergence speed and error metrics, validating its applicability for real-time robotic tasks [1,4,9,14].

5. CONCLUSIONS

This paper has presented a comprehensive framework for hybrid PID-feedforward control applied to trajectory tracking in two-degree-of-freedom (2-DOF) planar robotic manipulators, addressing the challenges posed by nonlinear dynamics such as inertial coupling, Coriolis effects, and gravitational torques. By deriving the system model through Euler-Lagrange equations and integrating a computed torque feedforward component with PID feedback, the proposed approach ensures precise compensation of nominal disturbances while correcting residual errors in real time. The control design, supported by Lyapunov-based stability analysis, guarantees asymptotic convergence of tracking errors under nominal conditions and bounded errors in the presence of model uncertainties, extending theoretical

foundations from prior works on hybrid systems [1,2,4,5,9]. Simulations conducted in MATLAB R2015a validated the method's efficacy, demonstrating root-mean-square (RMS) position errors of 0.5751° for the first joint and 1.4416° for the second under sinusoidal reference trajectories, with maximum errors limited to 5.36° and 28.65°, respectively. Compared to standalone PID control, the hybrid strategy reduced RMS errors by 45-60%, minimized actuator effort through torque decomposition (feedforward handling ~80% of the load), and maintained robustness in sensitivity tests with ±20% parameter variations, as evidenced by phase portraits, Cartesian paths, and moving RMS plots that showed rapid decay below 0.05° after initial transients [3,6,7,10,12].

The key contributions of this study include: (i) a tailored Lyapunov candidate incorporating integral action for enhanced stability proofs in multi-joint systems, (ii) detailed visualizations and metrics like torque breakdowns and configuration snapshots that quantify feedforward benefits, and (iii) practical extensions such as anti-windup mechanisms and empirical gain tuning, bridging gaps in literature focused on either purely adaptive or model-free methods [8,11,13,14]. These advancements not only improve tracking performance in simulated environments but also provide a scalable blueprint for industrial robotics, where energy efficiency and precision are paramount. However, limitations exist: the reliance on Euler integration may accumulate numerical errors in longer simulations, the model assumes rigid links without friction or backlash, and evaluations are confined to simulations without real-world disturbances like sensor noise or external forces [15]. Future research directions encompass experimental validation on physical prototypes, such as SCARA-like arms, incorporation of adaptive elements for online parameter estimation to handle uncertainties, and extension to higher-DOF systems or soft robotics, potentially integrating machine learning for gain optimization [2,5,9,12]. Overall, this work underscores the potential of hybrid controls to elevate robotic capabilities, fostering safer and more efficient human-robot collaborations in dynamic settings.

ACKNOWLEDGEMENTS

This study was supported by the Serbian Ministry of Science, Technological Development and Innovation from the grant 451-03-137/2025-03/200108.

REFERENCES

[1] H. T. T. Ngo, C. C. Nguyen, T. T. C. Duong, and T. T. Nguyen, "Trends in control strategies of parallel robot manipulators for robot-assisted rehabilitation", Engineering, Vol. 7(1), p. 44, https://doi.org/10.3390/eng7010044, (2026)

[2] E. A. Aner, O. M. Shehata, M. I. Awad, and N. E. ElHady, "A decade of soft robotic manipulators: Advances in design, modeling, control, and emerging challenges", Journal of Bionic Engineering, Vol. 23(1), pp. 55–98, https://doi.org/10.1007/s42235-025-00819-0, (2026)

[3] C. L. Nkwocha, A. Adewumi, S. O. Folorunsho, C. Eze, P. Jjagwe, J. Kemeshi, and N. Wang, "A comprehensive review of sensing, control, and networking in agricultural robots: From perception to coordination", Robotics, Vol. 14(11), p. 159, https://doi.org/10.3390/robotics14110159, (2025)

[4] C. D. Santina, R. K. Katzschmann, A. Bicchi, and D. Rus, "Model-based dynamic feedback control of a planar soft robot: Trajectory tracking and interaction with the environment", The International Journal of Robotics Research, Vol. 39(4), pp. 490–506, https://doi.org/10.1177/0278364919897292, (2020)

[5] A. M. Tusset, J. J. De Lima, F. C. Janzen, P. L. P. Filho, J. A. G. Luz Junior, J. M. Balthazar, and A. Kossoski, "A hybrid PID-LQR control applied in positioning control of robotic manipulators subject to excitation from non-ideal sources", Nonlinear Vibrations Excited by Limited Power Sources, Mechanisms and Machine Science, Vol. 116, pp. 321–328, https://doi.org/10.1007/978-3-030-96603-4_21, (2022)

[6] M. Wan, J. Dai, W. H. Zhang, Q.-B. Xiao, and X.-B. Qin, "Adaptive feed-forward friction compensation through developing an asymmetrical dynamic friction model", Mechanism and Machine Theory, Vol. 170, p. 104691, https://doi.org/10.1016/j.mechmachtheory.2021.104691, (2022)

[7] L. Zhang, J. Li, Y. Cui, M. Dong, B. Fang, and P. Zhang, "Design and performance analysis of a parallel wrist rehabilitation robot (PWRR)", Robotics and Autonomous Systems, Vol. 125, p. 103390, https://doi.org/10.1016/j.robot.2019.103390, (2020).

[8] Q. Xie, Q. Meng, Q. Zheng, Y. Fan, Y. Dai, and H. Yu, "Human-exoskeleton coupling dynamics of a multi-mode therapeutic exoskeleton for upper limb rehabilitation training", IEEE Access, Vol. 9, pp. 61998-62007, https://doi.org/10.1109/ACCESS.2021.3072781, (2021)

[9] V. Falkenhahn, A. Hildebrandt, R. Neumann, and O. Sawodny, "Dynamic control of the bionic handling assistant", IEEE/ASME Transactions on Mechatronics, Vol. 22(1), pp. 6–17, https://doi.org/10.1109/TMECH.2016.2605820, (2017)

[10] G. Grioli, W. Sebastian, M. Garabini, et al., "Variable stiffness actuators: The user's point of view", The International Journal of Robotics Research, Vol. 34(6), pp. 727–743, https://doi.org/10.1177/0278364914566515, (2015).

[11] W. S. Rone and P. Ben-Tzvi, "Continuum manipulator statics based on the principle of virtual work", Proceedings of the ASME 2012 International Mechanical Engineering Congress and Exposition. Vol. 4: Dynamics, Control and Uncertainty, Parts A and B, Houston, Texas (USA), pp. 321–328, https://doi.org/10.1115/IMECE2012-87675, (2012)

[12] P. Hyatt, D. Wingate, and M. D. Killpack, "Model-based control of soft actuators using learned non-linear discrete-time models", Frontiers in Robotics and AI, Vol. 6(22), https://doi.org/10.3389/frobt.2019.00022, (2019)

[13] T. G. Thuruthel, Y. Ansari, E. Falotico, and C. Laschi, "Control strategies for soft robotic manipulators: A survey", Soft Robotics, Vol. 5(2), pp. 149–163, https://doi.org/10.1089/soro.2017.0007, (2018)

[14] D. Rus and M. T. Tolley, "Design, fabrication and control of soft robots", Nature, Vol. 521, pp. 467–475, https://doi.org/10.1038/nature14543, (2015)

[15] N. Kellaris, V. G. Venkata, G. M. Smith, S. K. Mitchell, and C. Keplinger, "Peano-HASEL actuators: Muscle-mimetic, electrohydraulic transducers that linearly contract on activation", Science Robotics, Vol. 3(14), p. eaar3276, https://doi.org/10.1126/scirobotics.aar3276, (2018)